

Transport Phenomena in Two-Phase Micro-Channel Heat Sinks

Weilin Qu

Graduate Research Assistant,
Student Mem. ASME
e-mail: quw@purdue.edu

Issam Mudawar

Professor,
Fellow ASME
e-mail: mudawar@ecn.purdue.edu

Purdue University International Electronic
Cooling Alliance (PUIECA),
Boiling and Two-Phase Flow Laboratory,
School of Mechanical Engineering,
Purdue University,
West Lafayette, IN 47907

The design and reliable operation of a two-phase micro-channel heat sink require a fundamental understanding of the complex transport phenomena associated with convective boiling in small, parallel coolant passages. This understanding is the primary goal of this paper. This goal is realized by exploring the following aspects of boiling in micro-channels: hydrodynamic instability, two-phase flow patterns, pressure drop, and convective boiling heat transfer. High-speed photographic methods were used to determine dominant flow patterns and explore as well as characterize hydrodynamic instabilities. Two types of dynamic instability were identified, a severe pressure drop oscillation and a mild parallel channel instability, and a simple method is recommended to completely suppress the former. Predictions of three popular two-phase pressure drop models and correlations were compared to micro-channel water data, and only a separated flow (Lockhart-Martinelli) correlation based on the assumption of laminar flow in both phases gave acceptable predictions. Several popular heat transfer correlations were also examined and deemed unsuitable for micro-channel heat sinks because all these correlations are based on turbulent flow assumptions, and do not capture the unique features of micro-channel flow such as abrupt transition to slug flow, hydrodynamic instability, and high droplet entrainment in the annular regime. These findings point to the need for further study of boiling behavior and new predictive tools specifically tailored to micro-channel heat sinks. [DOI: 10.1115/1.1756145]

Introduction

The endless pursuit of denser circuit architecture has resulted in significant improvements in the performance of micro-electronic devices during the past three decades. Accompanying these improvements, however, has been a steady increase in heat generation at the component, module, and system levels, which is demanding more efficient electronic cooling technologies to ensure device reliability. Various innovative cooling schemes have been developed to meet this demand, which were recently reviewed by Mudawar [1]. Micro-channel heat sinks have been a prime contender for the next generation of high performance cooling systems. These heat sinks combine several attractive attributes, including the capability to dissipate very large heat fluxes from small areas, extremely compact dimensions, and small coolant inventory requirements.

Typically fabricated from a high thermal conductivity substrate, a micro-channel heat sink utilizes a series of small, parallel channels as coolant passages. A liquid coolant, such as water or a fluorochemical, is pumped through these passages, extracting heat from the device to which the heat sink is attached. The heat can be removed by simply increasing the temperature of the coolant through single-phase sensible heat exchange. Two-phase heat removal occurs when the coolant undergoes partial conversion to vapor. Two-phase heat sinks capitalize in part on the sensible heat exchange, but their effectiveness is derived mostly from latent heat exchange.

Single-phase micro-channel heat sinks have been studied quite extensively during the last two decades [2–10]. Not only did previous studies demonstrate the effectiveness of this cooling scheme, but they also provided fairly accurate modeling tools to describe both the pressure drop and heat transfer characteristics of the heat sink.

Phase change can greatly enhance the performance of a micro-

channel heat sink by providing higher convective heat transfer coefficients, better axial temperature uniformity, and reduced coolant flow rate requirements. Unfortunately, unlike their single-phase counterparts, the number of investigations into the fluid flow and heat transfer characteristics of two-phase micro-channel heat sinks is quite limited. Table 1 summarizes the present level of understanding of various aspects of single-phase and two-phase micro-channel heat sinks. Several representative studies on the latter are summarized below.

Boiling incipience in micro-channels was examined by Kennedy et al. [11] and Qu and Mudawar [12]. Kennedy et al. [11] studied incipient boiling of water flow in isolated micro-tubes with diameters of 1.17 and 1.45 mm. Significant deviation was found between experimental results for the smaller tube and predictions of classical correlations intended for macro systems. Qu and Mudawar [12] developed a mechanistic model to predict the incipient boiling heat flux in a heat sink containing $231 \times 713 \mu\text{m}^2$ micro-channels. Good agreement was found between the model predictions and experimental results for water over a broad range of flow rates and inlet temperatures.

Bowers and Mudawar [13–15] provided a comprehensive thermal design methodology for two-phase micro-channel heat sinks employing refrigerant coolants. A pressure drop model was constructed which incorporated the homogenous equilibrium model to describe the two-phase region. The model predictions were in good agreement with experimental results for R-113 in both mini-channel (2.54 mm) and micro-channel (510 μm) heat sinks. Their study also served to alert thermal design engineers to the unique challenges in predicting the performance of such heat sinks caused by compressibility, flashing, and even choking. These effects are the result of large axial property variations brought about by the relatively large micro-channel pressure drop.

Bubble activities and flow patterns in micro-channels were examined by Zhang et al. [16] and Jiang et al. [17]. Zhang et al. [16] studied boiling of water in isolated rectangular micro-channels with hydraulic diameters ranging from 25 to 60 μm , and aspect ratios from 1.0 to 3.5. Nucleation and growth of small

Contributed by the Electronic and Photonic Packaging Division for publication in the JOURNAL OF ELECTRONIC PACKAGING. Manuscript received April 2003; final revision, January 2004. Associate Editor: D. Agonafer.

Table 1 Current state of understanding of transport phenomena in micro-channel liquid heat sinks

Fluid State	Topic	Isolated Micro-channel	Parallel Micro-channels
Single-Phase Liquid	Laminar:	Adequate	Adequate
	Pressure drop	Adequate	Adequate
	Laminar:	Limited	Limited
	Heat transfer	Adequate	Adequate
	Transition	Adequate	Adequate
	Turbulent:	Adequate	Adequate
Two-phase	Pressure drop	Limited	Limited
	Turbulent:	Limited	Limited
	Heat transfer	Very limited	Very limited
	Incipient boiling	Limited	Limited
	Flow patterns	Limited	Limited
	Hydrodynamic instabilities	Very limited	Very limited
	Pressure drop	Limited	Limited
	Heat transfer	Limited	Limited
	Critical heat flux	Limited	Limited

bubbles were observed inside the micro-channels, but higher heat fluxes were associated with mostly annular two-phase flow. Jiang et al. [17] conducted flow visualization studies on water boiling in equilateral triangular micro-channel heat sinks with nominal widths of 50 μm and 100 μm . At low heat fluxes, individual bubbles were observed growing and departing inside the micro-channels. Increasing the heat flux triggered an abrupt transition in flow pattern to unstable slug flow, which was followed at higher heat fluxes by stable annular flow. Jiang et al. [17] never encountered the bubbly flow regime commonly observed in macro-channels.

Heat transfer characteristics of convective boiling in micro-channels were studied by Peng and Wang [18] and Ravigururajan [19]. Peng and Wang [18] investigated subcooled boiling of water through $600 \times 700 \mu\text{m}^2$ micro-channels. Their results revealed that, once initiated, nucleate boiling quickly becomes fully developed. Ravigururajan [19] studied convective boiling of R-124 in heat sinks containing parallel and diamond-oriented $270 \times 1000 \mu\text{m}^2$ micro-channels. The heat transfer coefficient decreased with increases in wall superheat and/or exit vapor quality.

Bowers and Mudawar [13,14] experimentally investigated critical heat flux (CHF) in mini-channel (2.54 mm) and micro-channel (510 μm) heat sinks and found that CHF values in excess of 200 W/cm^2 were possible with both heat sinks using R-113 as coolant and miniscule flow rates. Mudawar and Bowers [20] and Hall and Mudawar [21] investigated ultra-high CHF for water in small tubes with inner diameters ranging from 0.406 to 2.54 mm, and derived a correlation for a broad range of pressures, inlet temperatures, tube lengths, and flow rates. Their work culminated in the highest reported CHF value for water in a uniformly heated tube, 27,600 W/cm^2 .

While those and other investigations have provided valuable insight into the characterization and performance assessment of two-phase micro-channel heat sinks, the fundamental understanding of these devices remains quite limited. Virtually every aspect of two-phase fluid flow and heat transfer in a micro-channel seems to exhibit significant departure from macro-channel depictions. There are also vast differences in boiling behavior in micro-channels between water and fluorochemicals. Clearly, there is a shortage of reliable experimental databases and comprehensive modeling tools that can tackle the diversity of coolants, geometries, and operating conditions of micro-channel heat sinks.

In the present study, new experiments were conducted with a micro-channel heat sink using water as coolant, complementing earlier studies by the authors and co-workers. The experimental apparatus was configured for pressure drop and heat transfer measurements while providing visual access to the micro-channel flow. Based on the experimental results, several issues important to the implementation of micro-channel heat sinks are discussed;

namely, two-phase hydrodynamic instabilities, dominant two-phase flow patterns, pressure drop, and convective boiling heat transfer coefficient. The suitability of popular macro-channel two-phase models and correlations to depicting micro-channel flow is ascertained by comparing pressure drop and heat transfer coefficient predictions to experimental data.

Experimental Apparatus and Testing Procedure

Figure 1 shows a schematic diagram of the test facility. The flow loop in this facility delivered deionized water at the desired flow rate and inlet temperature to a test module containing the micro-channel heat sink. The flow loop consisted of a liquid reservoir, a variable-speed gear pump, a filter, two parallel rotameters, a constant temperature bath, the test module, and a water-cooled heat exchanger. Several throttling valves were incorporated in the flow loop to control the system pressure, and a pressure gauge was connected immediately downstream from the pump to monitor the pump's exit pressure. An immersion heater situated in the reservoir was used to both preheat and deaerate the water. The constant temperature bath brought the water to the desired test module inlet temperature, while the water-cooled heat exchanger condensed any vapor exiting the test module.

As shown in Fig. 2, the test module was composed of an oxygen-free-copper micro-channel heat sink, a G-7 fiberglass plastic housing, a transparent polycarbonate plastic (Lexan) cover plate, and twelve cartridge heaters. The micro-channel heat sink had a planform (top) area of 1.0 cm (width) by 4.48 cm (length). Twenty-one equidistant rectangular micro-slots, 231 μm wide and 712 μm deep, were machined along the top surface by a precision sawing technique. The surfaces of the slots were examined with the aid of a Nikon inverted metallurgical microscope, and the average surface roughness was estimated to be on the order of 1 μm . Three thin slots were cut from the bottom surface up through most of the heat sink's height to reduce heat spread within the heat sink and provide a more uniform heat flux distribution. The central portion of the housing was machined out where the micro-channel heat sink was inserted. The housing contained plenums both upstream and downstream. Each plenum had a deep portion leading to a shallow portion to ensure even distribution of flow between channels. The cover plate was bolted atop to form closed micro-channels. Twelve holes were drilled into the bottom of the copper heat sink to accommodate the cartridge heaters which provided the heat to the micro-channels. The cartridge heaters were powered by a single 0-110 VAC variac.

Two Type-K thermocouples were inserted into inlet and outlet plenums in the housing to measure the inlet and exit temperatures, respectively. Four additional Type-K thermocouples were inserted into the heat sink to measure the axial temperature distribution, and are indicated in Fig. 2 as *tc1* to *tc4* along the flow direction.

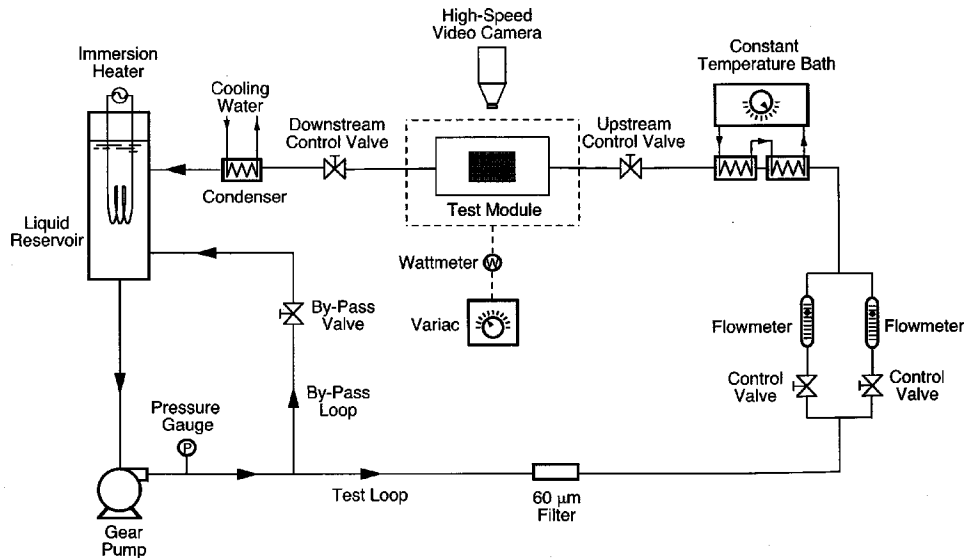


Fig. 1 Schematic diagram of low loop

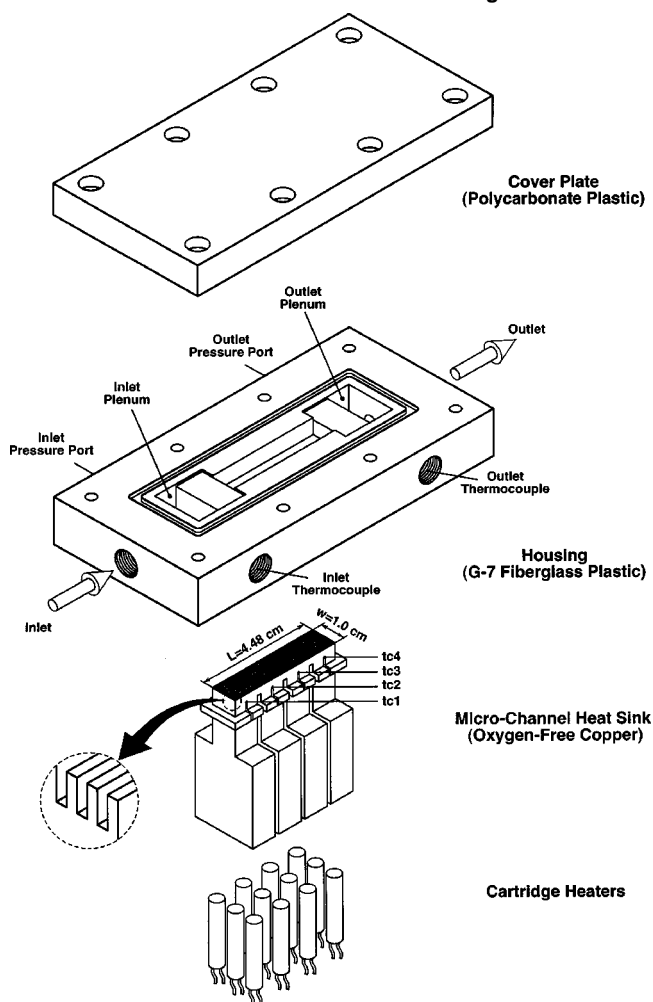


Fig. 2 Test module construction

Two absolute pressure transducers were connected to pressure taps in the deep portions of the housing plenums to measure the inlet and exit pressures. The thermocouple and pressure transducer signals were recorded by an HP data acquisition/control system which was interfaced to a PC.

After the test module was assembled, multiple layers of ceramic fiber were wrapped around the micro-channel heat sink for thermal insulation. A high-speed video camera was positioned above the transparent cover plate to monitor and record bubble behavior inside the channels.

The wattmeter used to measure the electrical power input to the cartridge heaters had an accuracy of 0.5%. Prior to performing flow boiling experiments, a series of single-phase heat transfer tests were conducted within the same flow rate range. Comparison between electronic power input and water enthalpy increase during the single-phase tests proved the total heat loss was less than 4%. All heat flux calculations in this study were therefore based on the electrical power input to the cartridge heaters. The rotameters were calibrated at the desired water temperature using the standard weighting method, and their flow rate measurement accuracy was better than 4%. The pressure transducers were calibrated against a known standard. The estimated uncertainty associated with the pressure measurements was less than 3.5%. Error associated with measurements of the calibrated thermocouples was smaller than $\pm 0.3^\circ\text{C}$.

The operating conditions of the present study are given in Table 2. Prior to performing a given test, the water in the reservoir was deaerated by vigorous boiling for about one hour to remove any dissolved gases which may cause early bubble formation within channels. The flow loop components were then adjusted to yield the desired operating conditions. In particular, the pump exit pressure, $P_{p,out}$, was elevated to 2.0 bar by throttling the control valve situated upstream of the test module. This helped dampen two-phase flow oscillations as will be discussed in a later section. The test commenced with single-phase liquid flow by setting the

Table 2 Operating conditions for present study

Coolant	Inlet temperature, T_{in} ($^\circ\text{C}$)	Mass velocity, G ($\text{kg}/\text{m}^2 \text{ s}$)	Outlet pressure, P_{out} (bar)	Pump exit pressure, $P_{p,out}$ (bar)
Deionized water	30.0	134.9–400.1	1.17	2.0
	60.0	134.9–401.9	1.17	2.0

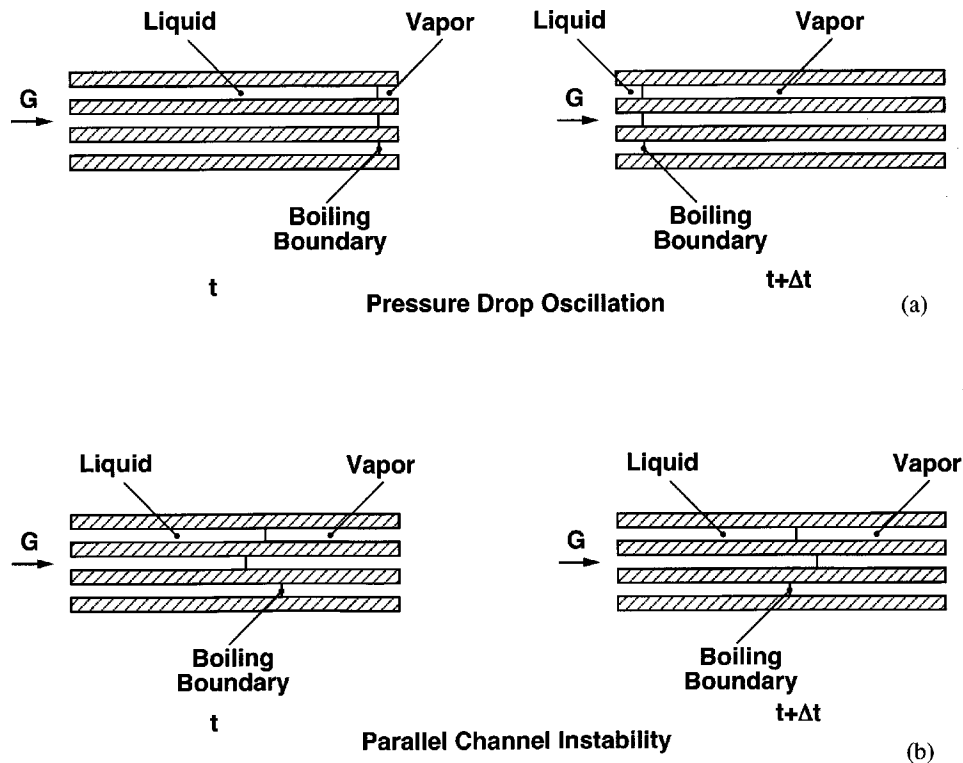


Fig. 3 Top views of micro-channels illustrating (a) pressure drop oscillation, (b) parallel channel instability

heater power below the incipient boiling condition. The power was then increased in small increments. At each new power level, the heat sink was allowed to reach steady state, which was confirmed when the mean pressures and temperatures became constant. After steady-state conditions prevailed, the inlet and outlet pressures, P_{in} and P_{out} , inlet and outlet temperatures, T_{in} and T_{out} , and heat sink temperatures, T_{tc1} to T_{tc4} , respectively, were all recorded at 0.5 s intervals for 5 min. These measured parameters were then time-averaged according to

$$\phi = \frac{1}{\tau} \int_0^{\tau} \phi_{inst} dt, \quad (1)$$

where ϕ represents the measured parameter, namely P or T , subscript *inst* indicates instantaneous value, and τ is the measurement period. Since the recording interval was constant (0.5 s), Eq. (1) was simplified as

$$\phi = \frac{1}{M} \sum \phi_{inst}, \quad (2)$$

where M is the number of data points recorded during a measurement period.

The test was terminated when the thermodynamic equilibrium quality,

$$x_e = \frac{h - h_f}{h_{fg}}, \quad (3)$$

reached about 0.2 at the channel exit.

Prior to conducting the final experiments, duplicate tests were performed for certain operating conditions. A consistent experimental procedure was adopted throughout the tests. The measured pressure drop and temperatures were virtually identical, validating the repeatability of experimental results.

Hydrodynamic Instabilities

Past research has revealed that various types of hydrodynamic instability exist in two-phase systems, and their physical origin varies significantly [22–24]. In general, two-phase instabilities are categorized as static or dynamic, depending on whether or not steady-state conservation laws can be applied to explain the instability. The two-phase static instabilities, such as flow excursion (Ledinegg instability) and flow pattern transition instability, are governed by steady-state conservation laws. On the other hand, the dynamic instabilities, such as acoustic oscillations, density wave oscillations, pressure drop oscillations, and parallel channel instability, involve transient inertia and dynamic feedback effects which cannot be described by steady-state conservation laws.

In the present two-phase micro-channel heat sink tests, two distinct types of dynamic instability were observed. The first type was encountered when the upstream control valve was fully open. As the heater power was gradually increased to the incipient boiling heat flux, nucleation sites started to appear within the micro-channels. A further increase in the heater power triggered an abrupt transition to intermittent two-phase flow. The boiling boundary (interface between the single-phase liquid region and two-phase mixture region) of all the channels oscillated back and forth in unison between channel inlet and outlet. A schematic of the flow oscillation within three neighboring channels for a short time interval (about 1 to 5 s) is illustrated in Fig. 3(a). For some cases, this oscillation was so severe that the vapor could enter the inlet plenum. During the oscillation, the inlet and exit pressures as well as the heat sink temperatures exhibited large amplitude fluctuations. The float in the rotameter also fluctuated appreciably, indicating the pump could not deliver a constant flow rate under these conditions. This instability may be classified as pressure drop oscillation, which is commonly triggered by flow excursion

and sustained by interactions between the vapor generation and the upstream compressible volume including the liquid reservoir and pump [23,24].

This pressure drop oscillation is very undesirable when operating a two-phase micro-channel heat sink, since it not only introduces large amplitude pressure and temperature fluctuations, but also reduces CHF. In fact, pre-mature CHF occurred at a much lower heat flux when the flow was undergoing pressure drop oscillation than when steady. Fortunately, the present experiments proved the pressure drop oscillation can be suppressed by throttling the control valve situated immediately upstream of the test module, which helped increase the system's stiffness. The upstream control valve was throttled until the pump exit pressure, $P_{p,out}$, reached 2.0 bar. Instead of the severe flow oscillation between the heat sink inlet and outlet, the boiling boundary was observed to fluctuate between micro-channels as illustrated in Fig. 3(b). The spatial amplitude of fluctuation around the mean axial position of the boiling boundary was reduced significantly in all micro-channels as indicated by the corresponding boiling boundaries in Figs. 3(a) and 3(b). The flow rate, pressures, and temperatures, were all fairly stable even at much higher heat input than with the pressure oscillation corresponding to a fully-open upstream control valve. Following Yudigaroglu's classification [24], this second type of "mild" hydrodynamic instability may be characterized as *parallel channel instability*, which was sustained by feedback effects between channels intrinsic to the heat sink.

Figures 4(a) and 4(b) show temporal records of inlet and outlet pressures recorded when the micro-channel heat sink is undergoing the pressure drop oscillation and the parallel channel instability, respectively. The operating conditions for the two situations are the same except for power input and the throttling of the upstream valve. Heat input to the heat sink is represented by an effective heat flux, q''_{eff} , defined as the total electrical power input divided by the heat sink top platform area. For the parallel channel instability, the upstream valve was throttled gradually until the pump exit pressure, $P_{p,out}$, reached 2.0 bar, which is about 0.5 bar higher than for the case of pressure drop oscillation corresponding to a fully-open valve. A much lower heat flux was applied in the pressure drop oscillation case to preclude pre-mature CHF. Eventhough the effective heat flux is about three times lower for the pressure drop oscillation case than for the parallel channel instability, the pressure fluctuations for the former are far more severe. Furthermore, the pressure fluctuations occurred at a fairly constant frequency for the former, while they were more random during the parallel channel instability. Similar conclusions can be drawn about channel wall temperature from the temporal records of heat sink thermocouples, Figs. 5(a) and 5(b), for the pressure oscillation and parallel channel instability, respectively.

All the results reported in the following sections were obtained with a throttled upstream control valve. While the severe pressure drop oscillation was prevented, the reported results were all subject to the mild parallel channel instability.

Two-Phase Flow Patterns

Recent studies by the authors have revealed a unique feature of water boiling in micro-channels which is not commonly encountered with micro-channel boiling of fluorochemicals (e.g., R-113 and FC-72) or boiling of water and other liquids in macro-channels. The relatively large surface tension and contact angle of water result in vapor bubbles whose departure diameter is often comparable to the channel characteristic dimension [12]. Therefore, the micro-channel wall will have a far more immediate and profound effect on bubble growth and coalescence in a micro-channel than in a large channel. One direct consequence of this phenomenon is that it is very difficult to sustain a *bubbly flow regime* in a micro-channel. Instead, transition to the *slug flow regime* occurs shortly after incipient boiling. For a multi-channel heat sink, flow patterns are also complicated by the parallel channel instability discussed in the previous section. For example, the

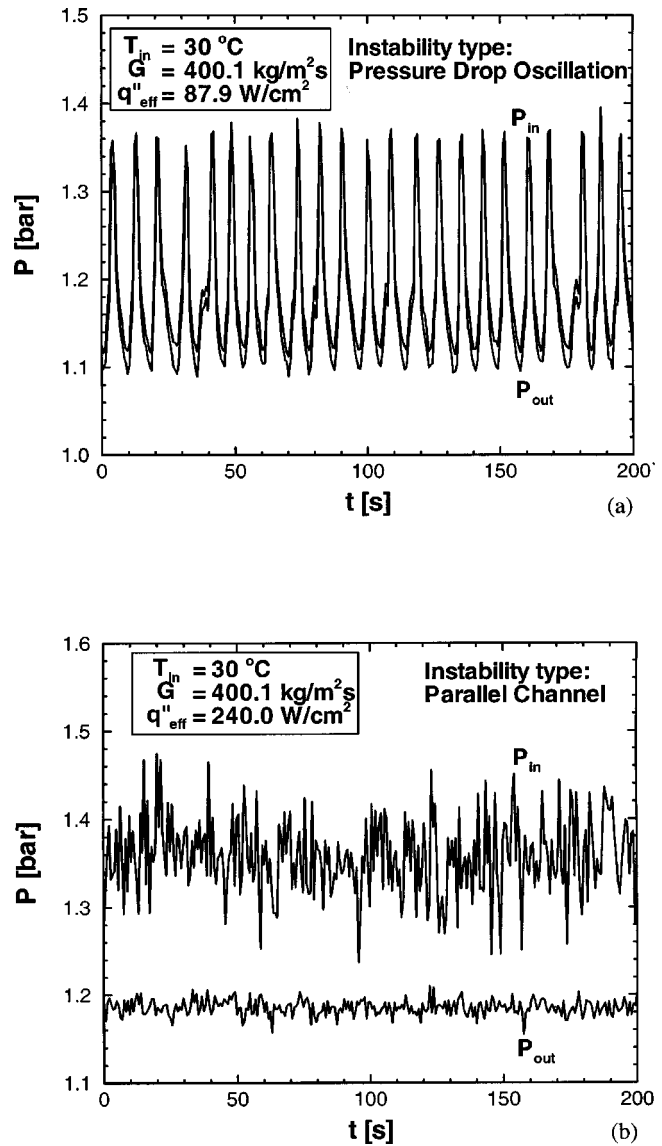


Fig. 4 Temporal records of inlet and outlet pressures during (a) pressure drop oscillation and (b) parallel channel instability

two-phase flow within an individual channel would oscillate between two distinct flow patterns even under constant operating conditions.

Flow patterns are also strongly influenced by the applied heat flux. Flow pattern transitions within an individual channel observed in the present study with increasing heat flux could be summarized as follows. At boiling incipience, illustrated schematically in Fig. 6(a), the flow consisted predominantly of single-phase liquid, except near the micro-channel exit, where a small number of nucleation sites appeared simultaneously in a few of the micro-channels. After nucleation, bubbles grew to their detachment size before being removed by the liquid flow. This process was repeated with the nucleation, growth and departure of newer bubbles.

When the heat flux was increased only slightly above the incipient boiling heat flux, boiling was visible within an increasing number of channels, and the boiling boundary moved further upstream. As illustrated in Fig. 6(b), a large number of nucleation sites were activated simultaneously within each channel. Those sites were typically located at the channel bottom wall near the corner. The bubbles grew until they coalesced with adjacent bubbles to form single oblong bubbles characteristic of the slug

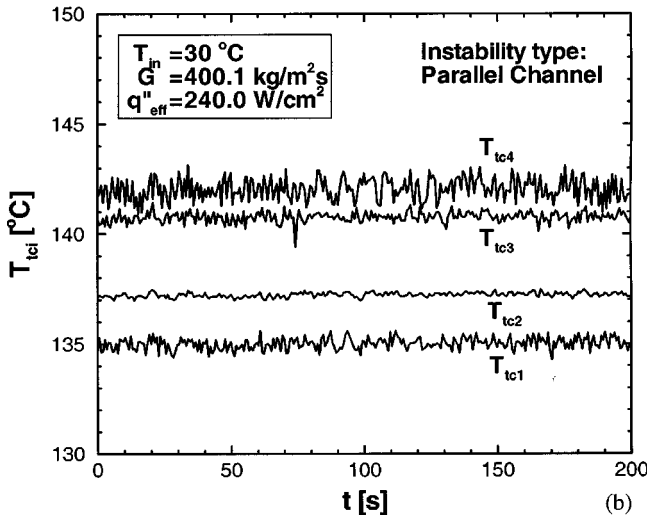
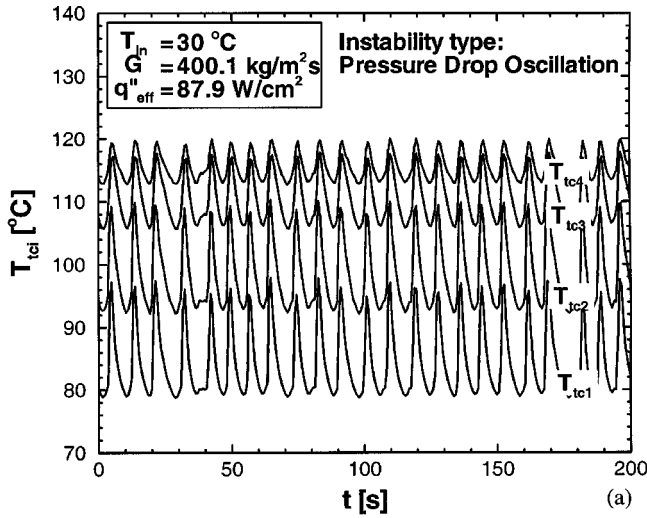


Fig. 5 Temporal records of heat sink temperatures during (a) pressure drop oscillation and (b) parallel channel instability

flow regime. The coalescent bubbles were quickly swept by the liquid to the downstream plenum, following which the entire process was repeated.

With a further increase in heat flux, the flow pattern was similar to that depicted in Fig. 6(b), except that the boiling boundary began to propagate closer to the channel inlet. More vapor bubbles were generated at the channel walls, which then coalesced to form two or three long slug bubbles along the channel. This pattern is depicted in Fig. 6(c).

At higher heat fluxes, the discrete bubbles were no longer observed. Instead, as illustrated in Fig. 6(d), the flow pattern oscillated between slug flow, with relatively short slug bubbles, and annular flow in the upstream region of the channel, while maintaining annular flow in the downstream region. A large number of liquid droplets were present in the downstream annular flow.

Pressure Drop

Pressure drop was determined by subtracting the measured outlet pressure from the measured inlet pressure. A pressure drop model of the heat sink must account for five distinct regions between the inlet and outlet pressure taps: inlet deep plenum, inlet

shallow plenum, micro-channels, outlet shallow plenum, and outlet deep plenum. Water was supplied in subcooled state ($T_{in} < T_{sat}$) for all test conditions as indicated in Table 2. Based on the magnitude of thermodynamic equilibrium quality, x_e , the micro-channels are divided into two regions: a single-phase region, from the subcooled inlet ($x_e < 0$) to the location where $x_e = 0$, and a two-phase region, from the location of zero quality to the heat sink exit ($x_e = x_{e,out}$), as illustrated in Fig. 7. The single-phase region is further divided into developing and fully-developed single-phase sub-regions. By neglecting pressure drop in the plenums, the total pressure drop can be expressed as

$$\Delta P = \Delta P_{c1} + \Delta P_{c2} + \Delta P_{sp,d} + \Delta P_{sp,f} + \Delta P_{tp} + \Delta P_{e2} + \Delta P_{e1}. \quad (4)$$

The individual component in Eq. (4) are evaluated as follows.

ΔP_{c1} and ΔP_{c2} are the contraction pressure losses from the deep plenum to the shallow plenum, and from the shallow plenum to the micro-channels, respectively. They are expressed as [25]

$$\Delta P_{c1} = \frac{1}{2v_f}(u_{p2,in}^2 - u_{p1,in}^2) + \frac{K_{c1}}{2v_f}u_{p2,in}^2, \quad (5)$$

and

$$\Delta P_{c2} = \frac{1}{2v_f}(u_{in}^2 - u_{p2,in}^2) + \frac{K_{c2}}{2v_f}u_{in}^2, \quad (6)$$

where subscripts $p1$ and $p2$ denote the deep plenum and shallow plenum, respectively, and K_{c1} and K_{c2} are the loss coefficients for the corresponding abrupt contractions.

Similarly, ΔP_{e2} and ΔP_{e1} are the expansion pressure recoveries from the micro-channels to the shallow plenum, and from the shallow plenum to the deep plenum, respectively, which are expressed as

$$\Delta P_{e2} = \frac{1}{2(v_f + x_{e,out}v_{fg})}(u_{p2,out}^2 - u_{out}^2) + \frac{K_{e2}}{2(v_f + x_{e,out}v_{fg})}u_{out}^2, \quad (7)$$

and

$$\Delta P_{e1} = \frac{1}{2(v_f + x_{e,out}v_{fg})}(u_{p1,out}^2 - u_{p2,out}^2) + \frac{K_{e1}}{2(v_f + x_{e,out}v_{fg})}u_{p2,out}^2, \quad (8)$$

where K_{e1} and K_{e2} are the recovery coefficients associated with the corresponding abrupt expansion. Values of K_{c1} , K_{c2} , K_{e1} and K_{e2} for the present heat sink geometry are evaluated in accordance with reference [25].

$\Delta P_{sp,d}$ and $\Delta P_{sp,f}$ are the pressure drops across the single-phase developing sub-region and fully developed sub-region, which can be expressed, respectively, as

$$\Delta P_{sp,d} = \frac{2f_{app}G^2L_{sp,d}v_f}{d_h} \quad (9)$$

and

$$\Delta P_{sp,f} = \frac{2fG^2L_{sp,f}v_f}{d_h}. \quad (10)$$

For the range of flow rate tested in the present study, the upstream single-phase flow remained in the laminar regime ($Re_{dh} < 2300$). Methods to evaluate the pressure drops for developing and fully-developed single-phase sub-regions of a rectangular channel have been well documented by Shah and London [26]. Therefore, details of the development length, $L_{sp,d}$, apparent friction factor for the developing sub-region, f_{app} , and friction factor for the fully-developed region, f , have been left out of the present paper.

The pressure drop across the two-phase region consists of two components: frictional and accelerational.

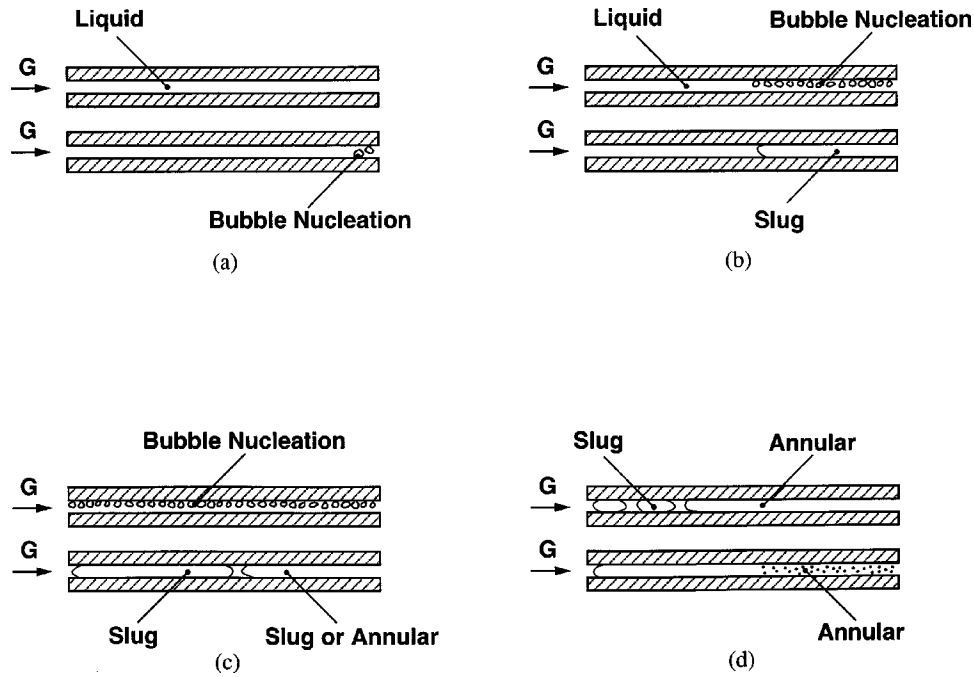


Fig. 6 Dominant two-phase flow patterns at (a) incipient boiling heat flux, (b) slightly above incipient boiling heat flux, (c) low heat flux, and (d) high heat flux

$$\Delta P_{tp} = \Delta P_{tp,f} + \Delta P_{tp,a} \quad (11)$$

The frictional pressure drop $\Delta P_{sp,f}$ is the result of wall frictional forces exerted upon the flow, and the accelerational pressure drop $\Delta P_{sp,a}$ is the result of axial acceleration of the two-phase mixture due to the conversion of liquid to vapor. A large number of models are available in the literature to evaluate $\Delta P_{sp,f}$ and $\Delta P_{sp,a}$ for convective boiling in large channels, which include generalized models without reference to a specific flow pattern, and correlations developed for a particular flow pattern. In the present study, three widely used generalized models, namely, the homogeneous equilibrium model (HEM) [27], Martinelli-Nelson (M-N) correlation [28], and Lockhart-Martinelli (L-M) correlation [29,30], are employed to evaluate the two-phase pressure drop. All relevant equations of these three models are given in Table 3. When applying the Lockhart-Martinelli correlation, the laminar liquid-laminar vapor combination was adopted for frictional pressure

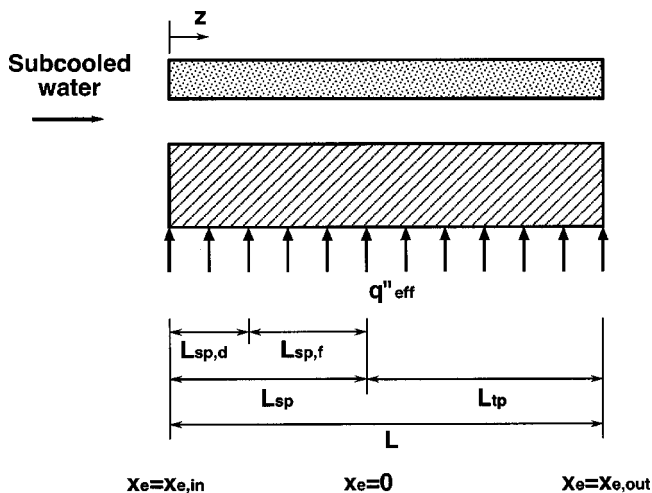


Fig. 7 Schematic of flow regions in a micro-channel

drop, $\Delta P_{sp,f}$, evaluation since the Reynolds numbers based on each of the liquid and vapor flow rates was less than 2000 for the operating conditions of the present study.

Figures 8(a) and 8(b) show both measured and predicted pressure drop as a function of heat flux for the same mass velocity and two inlet temperatures of 30 and 60°C, respectively. The pressure drop is fairly constant at small heat flux values, where the flow consists entirely of single-phase liquid. Once boiling is initiated, the pressure drop begins to rise appreciably with increasing heat flux. These figures show the homogeneous equilibrium model and Martinelli-Nelson correlation overpredict the pressure drop by large margins. Far better predictions are achieved with the Lockhart-Martinelli correlation at both inlet temperatures. The superior predictive capability of the Lockhart-Martinelli correlation is further demonstrated in Fig. 9, which contains all the pressure drop data obtained in the present study.

It should be noted that both the Martinelli-Nelson correlation and Lockhart-Martinelli correlation share the same development rationale. However, the Martinelli-Nelson correlation is based on the assumption of a turbulent liquid-turbulent vapor flow combination, since this combination is more prevalent in macro-channels, while the Lockhart-Martinelli correlation can account for different combinations of liquid-vapor flow (turbulent-turbulent, turbulent-laminar, laminar-turbulent, and laminar-laminar). Figures 8(a) and 8(b) reveal correlations based on turbulent liquid or turbulent vapor flow may not be appropriate for micro-channels, where low coolant flow rate and small channel size produce predominantly laminar flow for both phases.

Another interesting result of the present pressure model and correlation assessment is the failure of the homogeneous equilibrium model at predicting the present water micro-channel data, when the same model yielded accurate predictions of Bowers and Mudawar's pressure drop data for R-113 boiling in a heat sink containing 510 μm circular micro-channels [13-15]. This apparent discrepancy can be explained by fundamental differences in boiling behavior between water and R-113. The latter refrigerant features low surface tension and small contact angle, which result in bubble departure diameters one or two orders of magnitude smaller than those for water. These differences greatly influence

Table 3 Pressure drop models and correlations employed in describing the two-phase region

Homogeneous equilibrium model (HEM) [15,27]	$\Delta P_{ip,f} = \frac{2 f_{ip} G^2 L_{ip} v_f}{d_h} \left[1 + \frac{x_{e,out}}{2} \left(\frac{v_{fg}}{v_f} \right) \right]$ $f_{ip} = 0.003$ $\Delta P_{ip,a} = G^2 v_f x_{e,out}$
Martinelli-Nelson (M-N) correlation [28]	$\Delta P_{ip,f} = \frac{2 f G^2 L_{ip} v_f}{d_h} r_1(x_{e,out}, P)$ $r_1(x_{e,out}, P): \text{ from Fig. 4 in reference [28]}$ $\Delta P_{ip,a} = G^2 v_f r_2(x_{e,out}, P)$ $r_2(x_{e,out}, P): \text{ from Fig. 6 in reference [28]}$
Lockhart-Martinelli (L-M) correlation [29,30]	$\Delta P_{ip,f} = \frac{L_{ip}}{x_{e,out}} \int_0^{x_{e,out}} \frac{2 f_f G^2 (1-x_e)^2 v_f}{d_h} \phi_f^2 dx_e$ $f_f = \frac{24(1 - 1.355\beta + 1.947\beta^2 - 1.701\beta^3 + 0.956\beta^4 - 0.254\beta^5)}{G(1-x_e)d_h}$ $\phi_f^2 = 1 + \frac{C}{X_{vv}} + \frac{1}{X_{vv}^2}$ $C = 5$ $X_{vv} = \left(\frac{\mu_f}{\mu_g} \right)^{0.5} \left(\frac{1-x_e}{x_e} \right)^{0.5} \left(\frac{v_f}{v_g} \right)^{0.5}$ $\Delta P_{ip,a} = G^2 v_f \left[\frac{x_{e,out}^2}{\alpha_{out}} \left(\frac{v_g}{v_f} \right) + \frac{(1-x_{e,out})^2}{1-\alpha_{out}} - 1 \right]$ $\alpha_{out} = 1 - \frac{1}{\sqrt{1 + \frac{20}{X_{vv,out}} + \frac{1}{X_{vv,out}^2}}}$

both the dominant two-phase flow patterns and the transitions between flow patterns, and therefore must have a strong bearing on the two-phase pressure drop. Recently, Mukherjee and Mudawar [31] experimentally demonstrated the same differences in boiling behavior between water and FC-72 in narrow and micro-channels; FC-72 is a fluorochemical coolant with thermophysical properties similar to those of refrigerants. Their experiments showed the small surface tension and contact angle of FC-72 produce very small bubbles that could easily pass through small channels, while much larger bubbles in water obstructed liquid replenishment in identical channels.

Heat Transfer Coefficient

The heat transfer coefficient, averaged over the heated perimeter of the micro-channel, was evaluated at four axial locations where the thermocouple measurements were made, z_{tc1} , z_{tc2} , z_{tc3} , and z_{tc4} . Calculation of the average heat transfer was based on the fin analysis method, where the solid walls separating micro-channels are modeled as thin fins. Application of this method to evaluate the heat transfer coefficient in single-phase micro-channel heat sinks was discussed in detail by Qu and Mudawar [32]. This method adopts specific approximations such as one-dimensional heat transfer along the fins, constant convective heat transfer coefficient, and uniform fluid temperature, to model the conjugate heat transfer in the heat sink's cross-section at any given axial location z .

A two-dimensional micro-channel heat sink unit cell containing a single micro-channel and surrounding solid is examined at each thermocouple location as shown in Fig. 10. Dimensions of the unit cell are given in Table 4. In Fig. 10, T_{tci} ($i = 1, 2, 3, 4$) denotes the thermocouple temperature measured experimentally by thermocouple tci . Assuming one-dimensional heat diffusion between the thermocouple and the channel bottom wall, the temperature of the channel bottom wall, $T_{w,tci}$, can be expressed as

$$T_{w,tci} = T_{tci} - \frac{q''_{eff} H_{w2}}{k_s} \quad (12)$$

Axial variations of the mean flow temperature $T_{m,tci}$ can be explained by referring to Fig. 7. If the thermocouple is located within the single-phase region ($z_{tci} \leq L_{sp}$), $T_{m,tci}$ can be determined by a simple sensible energy balance.

$$\rho_f c_p v_f u_{in} A_c (T_{m,tci} - T_{in}) = q''_{eff} W_{cell} z_{tci} \quad (13)$$

Otherwise, if the thermocouple is located within the two-phase region ($L_{sp} \leq z_{tci} \leq L$), $T_{m,tci}$ is set equal to the saturation temperature.

$$T_{m,tci} = T_{sat} \quad (14)$$

By neglecting heat loss from the insulating plastic cover plate, the following energy balance can be written for the unit cell

$$q''_{eff} W_{cell} = h_{ave} (T_{w,tci} - T_{m,tci}) (W_{ch} + 2 \eta H_{ch}) \quad (15)$$

The left hand side of Eq. (15) represents the heat input to the unit cell and the right hand side the heat removal by convective heat transfer from the channel walls. The thin fin approximation is applied to the channel side walls by introducing the fin efficiency η ,

$$\eta = \frac{\tanh(m H_{ch})}{m H_{ch}} \quad (16)$$

where m is the fin parameter,

$$m = \sqrt{\frac{h_{ave}}{k_s W_w}} \quad (17)$$

Once $T_{w,tci}$ and $T_{m,tci}$ are determined from Eqs. (12) to (14), the value of the average heat transfer coefficient h_{ave} can be readily calculated from Eq. (15).

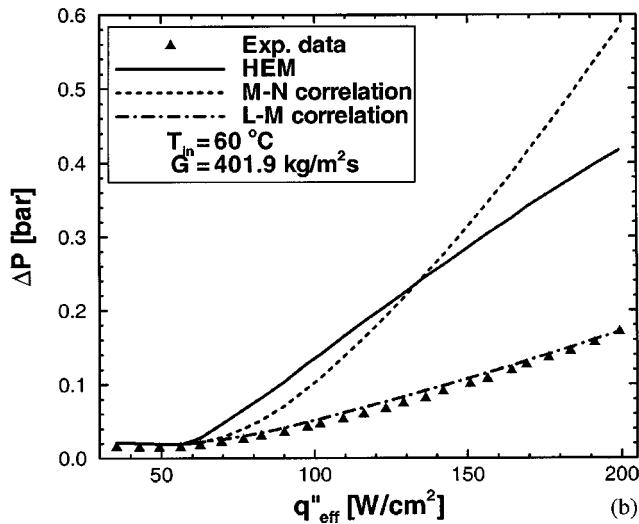
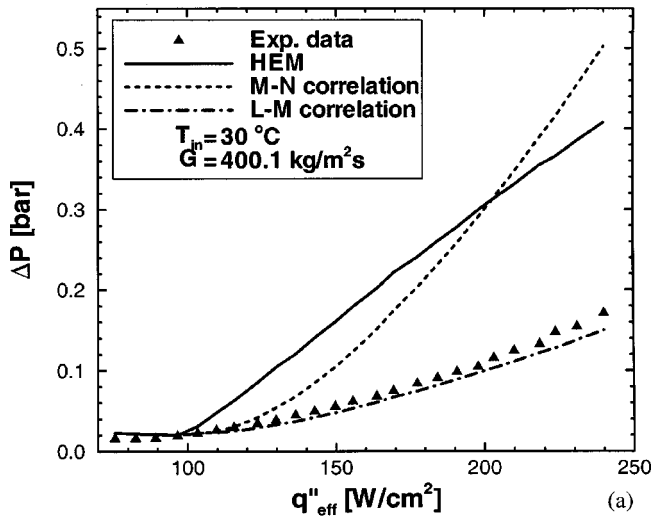


Fig. 8 Comparison of pressure drop data and predictions at $G=400 \text{ kg/m}^2\text{s}$ for (a) $T_{in}=30^\circ\text{C}$ and (b) $T_{in}=60^\circ\text{C}$

Figures 11(a) and 11(b) show the measured average heat transfer coefficient h_{ave} as a function of thermodynamic equilibrium quality x_e at each thermocouple location for the same mass velocity and inlet temperatures of 30 and 60°C, respectively. Three regions featuring drastically different heat transfer characteristics can be readily identified. To the left end of each plot, the h_{ave} values are small and fairly constant, indicative of single-phase liquid flow. This is followed by a region of sharp rise in the heat transfer coefficient until the thermodynamic equilibrium quality, x_e , reaches zero. This is characteristic of the subcooled boiling region where the heat transfer is greatly enhanced. The third region to the right side of $x_e=0$ corresponds to saturated boiling. Figures 11(a) and 11(b) show the average heat transfer coefficient is much larger in the two-phase region than in the single-phase region, which is further proof of the superior cooling performance of two-phase micro-channel heat sinks over their single-phase counterparts. In the saturated boiling region ($x_e>0$), h_{ave} begins decreasing, which is consistent with the observations of Ravigururajan [19]. The higher heat transfer near $x_e=0$ may be caused by entrance or hydrodynamic instability effects, and is the subject of further investigation.

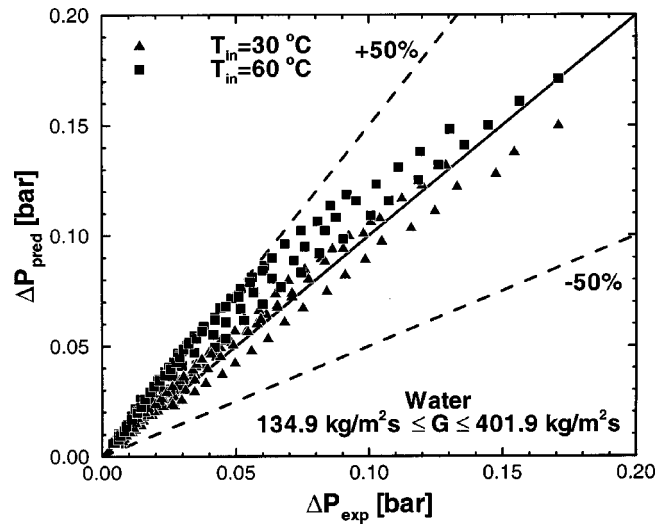


Fig. 9 Comparison of pressure drop data and predictions based on Lockhart-Martinelli correlation

Five widely used two-phase heat transfer coefficient correlations, Chen [33,34], Shah [35,36], Kandlikar [37], Liu-Winterton [38], and Steiner-Taborek [39], were examined in predicting the saturated convective boiling heat transfer coefficient at z_{tc4} , the thermocouple location closest to the channel exit. Figures 12(a) and 12(b) compare the experimental results to the predictions of the five correlations for inlet temperatures of 30 and 60°C, re-

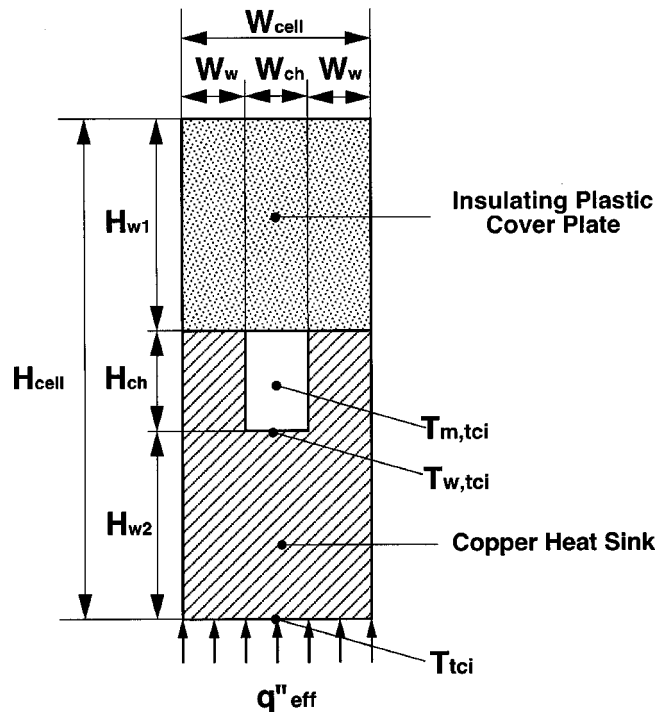


Fig. 10 Schematic of micro-channel heat sink unit cell

Table 4 Dimensions of micro-channel heat sink unit cell

W_w (μm)	W_{ch} (μm)	H_{w1} (μm)	H_{ch} (μm)	H_{w2} (μm)
118	231	12,700	713	2462

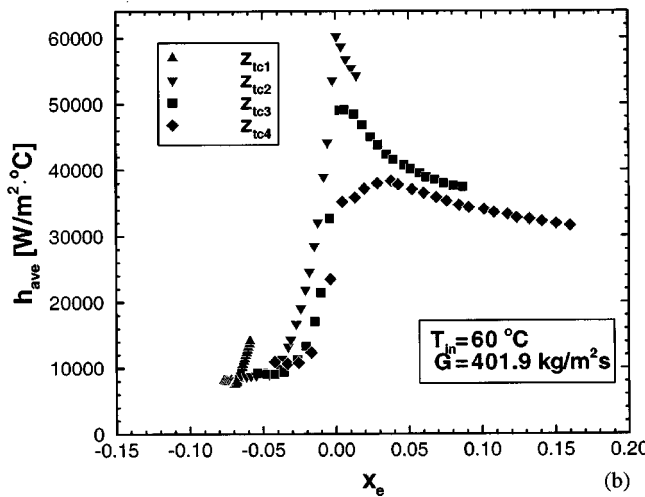
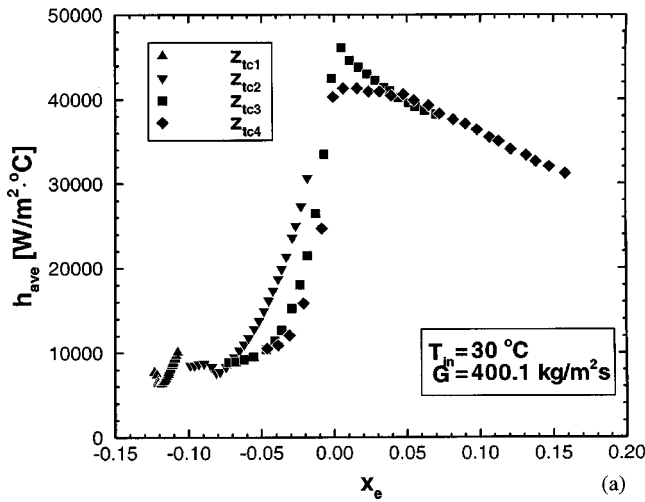


Fig. 11 Average heat transfer coefficient versus thermodynamic equilibrium quality at $G=400 \text{ kg/m}^2\text{s}$ for (a) $T_{in}=30^\circ\text{C}$ and (b) $T_{in}=60^\circ\text{C}$

spectively. Shown is a noticeable departure of all predictions from the measured variation of heat transfer coefficient with thermodynamic equilibrium quality.

The deviation between the predictions of all five correlations and the present experimental results can be attributed to several factors. First, all the aforementioned correlations were based on turbulent heat transfer coefficient correlations, such as the Dittus-Boelter equation, which are not valid for micro-channel flows. In fact, the Reynolds number Re_{in} based on inlet liquid flow rate and properties for the present study range from 60 to 300, for which the applicability of turbulent heat transfer correlations is highly questionable. This is the same reason the Martinelli-Nelson correlation yielded poor predictions of two-phase pressure drop.

Other unique features of boiling in micro-channel heat sinks, such as the abrupt transition to slug flow, hydrodynamic instability, and large number of liquid droplets entrained in the annular flow, may have contributed greatly to the deviation between data and predictions. Future studies should explore these issues more thoroughly in pursuit of a better fundamental understanding of boiling in micro-channel heat sinks. Such efforts are necessary steps towards developing more reliable predictive tools for micro-channel heat sink design.

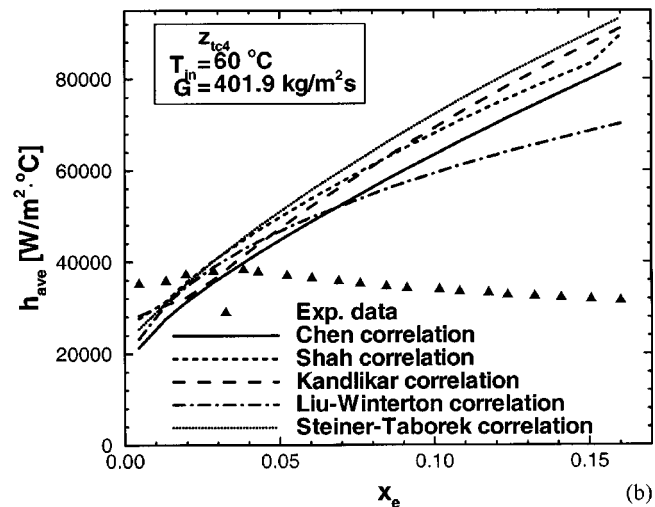
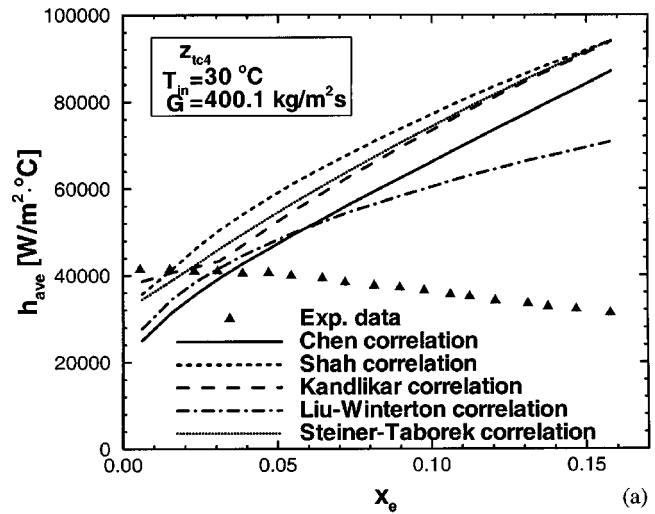


Fig. 12 Comparison of saturated convective boiling heat transfer coefficient data and predictions at $G=400 \text{ kg/m}^2\text{s}$ for (a) $T_{in}=30^\circ\text{C}$ and (b) $T_{in}=60^\circ\text{C}$

Conclusions

This paper explored several aspects of fluid flow and heat transfer in two-phase micro-channel heat sinks. Two key goals of the study were to identify the fundamental differences between two-phase flow in a micro-channel heat sink and macro-channels, and to assess the suitability of popular macro-channel models and correlations at predicting two-phase pressure drop and saturated convective boiling heat transfer in micro-channel heat sinks. Key conclusions from the study are as follows:

1. Two types of two-phase dynamic instability were identified, pressure drop oscillation and parallel channel instability. Pressure drop oscillation was associated with fairly periodic, large-amplitude fluctuations in inlet and outlet pressure as well as heat sink temperature. This type of instability was completely suppressed by throttling a control valve situated upstream of the heat sink. Parallel channel instability produced only mild fluctuations in the pressure and temperature.
2. Following the onset of boiling, bubbles quickly coalesced into oblong bubbles typical of slug flow. High fluxes produced

mostly annular flow. Parallel channel instability caused the flow in an individual channel to oscillate between different flow patterns even at constant operating conditions.

3. Pressure drop across the heat sink was fairly constant with increasing heat flux for single-phase liquid flow, but increased appreciably when boiling commenced inside the micro-channels. A pressure drop model was constructed, which accounts for single-phase and two-phase regions, as well as inlet contraction pressure loss and exit expansion recovery. Three popular techniques were examined in modeling the two-phase region, the homogeneous equilibrium model, the Martinelli-Nelson correlation, and the Lockhart-Martinelli correlation. The latter yielded the best agreement with the experimental data.

4. While the homogeneous equilibrium has yielded accurate pressure drop predictions in past studies of micro-channel heat sinks employing fluorochemical liquids, this model gave poor predictions of the present water data. This apparent discrepancy seems to be caused by the relatively large bubble departure in water engulfing the entire cross-section and causing abrupt transition to the slug flow regime. In fluorochemical coolants, low surface tension and small contact angle produce much smaller bubbles, a fairly well-developed bubbly flow regime, and a smoother transition into the slug flow regime.

5. Three regions with drastically different heat transfer characteristics were identified: single-phase, subcooled boiling, and saturated boiling. The heat transfer is significantly enhanced in the two-phase region. Several popular correlations were examined and deemed unsuitable at predicting the heat transfer coefficient in the saturated boiling region. The deviation between the predictions and experimental data is attributed to the turbulent flow assumption employed in all these correlations, and to unique features of two-phase micro-channel heat sinks such as abrupt transition to slug flow, hydrodynamic instability, and large number of liquid droplets entrained in the annular flow. These results point to the need for further study of boiling behavior in micro-channel heat sinks, and for new predictive tools specifically tailored to micro-channel flow.

Acknowledgment

The authors are grateful for the support of the Office of Basic Energy Sciences of the U.S. Department of Energy (Award No. DE-FG02-93ER14394-A7).

Nomenclature

A_c	= cross-sectional area of micro-channel
C	= empirical constant in Martinelli parameter X_{vv}
c_p	= specific heat at constant pressure
d_h	= hydraulic diameter of micro-channel
f	= friction factor for fully-developed single-phase liquid flow
f_{app}	= apparent friction factor for developing single-phase liquid flow
f_f	= friction factor based on local liquid flow rate
f_{ip}	= two-phase friction factor
G	= mass velocity
h_{ave}	= average convection heat transfer coefficient
h_f	= enthalpy of saturated liquid
h_{fg}	= latent heat of vaporization
H_{cell}	= height of unit cell
H_{ch}	= height of micro-channel
H_{w1}	= thickness of plastic cover plate
H_{w2}	= distance from thermocouple to micro-channel bottom wall
k	= thermal conductivity
K_{c1}, K_{c2}	= contraction loss coefficient
K_{e1}, K_{e2}	= expansion recovery coefficient
L	= length of micro-channel
L_{sp}	= length of single-phase region

$L_{sp,d}$	= length of single-phase developing sub-region
$L_{sp,f}$	= length of single-phase fully-developed sub-region
L_{ip}	= length of two-phase region
m	= fin parameter
M	= number of data points recorded during a measurement period
P	= pressure
P_{in}	= inlet pressure
P_{out}	= outlet pressure
$P_{p,out}$	= pump exit pressure
ΔP	= total pressure drop
$\Delta P_{c1}, \Delta P_{c2}$	= contraction pressure loss
$\Delta P_{e1}, \Delta P_{e2}$	= expansion pressure loss
$\Delta P_{sp,d}$	= pressure drop in single-phase developing sub-region
$\Delta P_{sp,f}$	= pressure drop in single-phase fully-developed sub-region
ΔP_{ip}	= pressure drop in two-phase region
$\Delta P_{ip,a}$	= accelerational two-phase pressure drop
$\Delta P_{ip,f}$	= frictional two-phase pressure drop
q_{eff}	= heat flux based on heat sink top planform area
r_1, r_2	= coefficients in Martinelli-Nelson correlation
Re_{dh}	= Reynolds number of micro-channel based on inlet liquid flow rate and properties
t	= time
T	= temperature
T_{in}	= micro-channel inlet temperature
$T_{m,tc1}$	= mean flow temperature at thermocouple location
T_{out}	= micro-channel outlet temperature
T_{sat}	= saturation temperature
T_{tc1}	= thermocouple reading ($i=1$ to 4)
$T_{w,tc1}$	= channel bottom wall temperature at thermocouple location
u_{in}	= inlet velocity
u_{out}	= outlet velocity
v	= specific volume
v_{fg}	= specific volume difference between saturated vapor and saturated liquid
W	= width of heat sink top planform area
W_{cell}	= width of unit cell
W_{ch}	= width of micro-channel
W_w	= half-width of wall separating micro-channels
x_e	= thermodynamic equilibrium quality
$x_{e,out}$	= thermodynamic equilibrium quality at channel outlet
X_{vv}	= Martinelli parameter for laminar liquid-laminar vapor flow
z	= axial coordinate
z_{tc1}	= axial location of thermocouple ($i=1$ to 4)

Greek Symbols

α	= void fraction
β	= aspect ratio
ϕ	= measured parameter
ϕ_f^2	= two-phase frictional multiplier based on local liquid flow rate
η	= fin efficiency
μ	= viscosity
ρ	= density
τ	= measurement period

Subscripts

ave	= average
exp	= experimental (measured)
f	= liquid
g	= vapor
in	= inlet

inst = instantaneous
out = outlet
pred = predicted
p1 = deep plenum
p2 = shallow plenum
s = solid (oxygen-free copper)
sp = single-phase
tc = thermocouple
tp = two-phase.

References

- [1] Mudawar, I., 2001, "Assessment of High-Heat-Flux Thermal Management Schemes," *IEEE Trans. Compon., Packag. Manuf. Technol., Part A*, **24**, pp. 122–141.
- [2] Tuckerman, D. B., and Pease, R. F. W., 1981, "High-Performance Heat Sinking for VLSI," *IEEE Electron Device Lett.*, **EDL-Vol. 2**, pp. 126–129.
- [3] Phillips, R. J., 1990, "Micro-Channel Heat Sinks," *Advances in Thermal Modeling of Electronic Components*, A. Bar-Cohen, and A. D. Kraus, eds., ASME Press, New York, **2**, pp. 109–184.
- [4] Knight, R. W., Hall, D. J., Goodling, J. S., and Jaeger, R. C., 1992, "Heat Sink Optimization with Application to Microchannels," *IEEE Trans. Compon., Hybrids, Manuf. Technol.*, **15**, pp. 832–842.
- [5] Weisberg, A., Bau, H. H., and Zemel, J. N., 1992, "Analysis of Microchannels for Integrated Cooling," *Int. J. Heat Mass Transfer*, **35**, pp. 2465–2474.
- [6] Kawano, K., Minakami, K., Iwasaki, H., and Ishizuka, M., 1998, "Micro Channel Heat Exchanger for Cooling Electrical Equipment," *Proceedings of the ASME Heat Transfer Division*, R. A. Nelson et al., eds., ASME, HTD-Vol. 361-3/PID-Vol. 3, pp. 173–180.
- [7] Harms, T. M., Kazmierczak, M. J., and Cerner, F. M., 1999, "Developing Convective Heat Transfer in Deep Rectangular Microchannels," *Int. J. Heat Fluid Flow*, **20**, pp. 149–157.
- [8] Fedorov, A. G., and Viskanta, R., 2000, "Three-Dimensional Conjugate Heat Transfer in the Microchannel Heat Sink for Electronic Packaging," *Int. J. Heat Mass Transfer*, **43**, pp. 399–415.
- [9] Qu, W., and Mudawar, I., 2002, "Analysis of Three-Dimensional Heat Transfer in Micro-Channel Heat Sinks," *Int. J. Heat Mass Transfer*, **45**, pp. 3973–3985.
- [10] Qu, W., and Mudawar, I., 2002, "Experimental and Numerical Study of Pressure Drop and Heat Transfer in a Single-Phase Micro-Channel Heat Sink," *Int. J. Heat Mass Transfer*, **45**, pp. 2549–2565.
- [11] Kennedy, J. E., Roach, Jr., G. M., Dowling, M. F., Abdel-Khalik, S. I., Ghiaasiaan, S. M., Jeter, S. M., and Quershi, Z. H., 2000, "The Onset of Flow Instability in Uniformly Heated Horizontal Microchannels," *ASME J. Heat Transfer*, **122**, pp. 118–125.
- [12] Qu, W., and Mudawar, I., 2002, "Prediction and Measurement of Incipient Boiling Heat Flux in Micro-Channel Heat Sinks," *Int. J. Heat Mass Transfer*, **45**, pp. 3933–3945.
- [13] Bowers, M. B., and Mudawar, I., 1994, "High Flux Boiling in Low Flow Rate, Low Pressure Drop Mini-Channel and Micro-Channel Heat Sinks," *Int. J. Heat Mass Transfer*, **37**, pp. 321–332.
- [14] Bowers, M. B., and Mudawar, I., 1994, "Two-Phase Electronic Cooling Using Mini-Channel and Micro-Channel Heat Sinks: Part 1-Design Criteria and Heat Diffusion Constraints," *ASME J. Electron. Packag.*, **116**, pp. 290–297.
- [15] Bowers, M. B., and Mudawar, I., 1994, "Two-Phase Electronic Cooling Using Mini-Channel and Micro-Channel Heat Sinks: Part 2-Flow Rate and Pressure Drop Constraints," *ASME J. Electron. Packag.*, **116**, pp. 298–305.
- [16] Zhang, L., Koo, J. M., Jiang, L., Banerjee, S. S., Ashghi, M., Goodson, K. E., Santiago, J. G., and Kenny, T. W., 2000, "Measurement and Modeling of Two-Phase Flow in Microchannels with Nearly-Constant Heat Flux Boundary Conditions," *Micro-Electro-Mechanical Systems (MEMS)-2000*, A. Lee et al., eds., ASME, MEMS-Vol. 2, pp. 129–135.
- [17] Jiang, L., Wong, M., and Zohar, Y., 2001, "Forced Convection Boiling in a Microchannel Heat Sink," *J. Microelectromech. Syst.*, **10**, pp. 80–87.
- [18] Peng, X. F., and Wang, B. X., 1993, "Forced Convection and Flow Boiling Heat Transfer for Liquid Flowing through Microchannels," *Int. J. Heat Mass Transfer*, **36**, pp. 3421–3427.
- [19] Ravigurajan, T. S., 1998, "Impact of Channel Geometry on Two-Phase Flow Heat Transfer Characteristics of Refrigerants in Microchannel Heat Exchangers," *ASME J. Heat Transfer*, **120**, pp. 485–491.
- [20] Mudawar, I., and Bowers, M. B., 1999, "Ultra-High Critical Heat Flux (CHF) for Subcooled Water Flow Boiling—I: CHF Data and Parametric Effects for Small Diameter Tubes," *Int. J. Heat Mass Transfer*, **42**, pp. 1405–1428.
- [21] Hall, D. D., and Mudawar, I., 1999, "Ultra-High Critical Heat Flux (CHF) for Subcooled Water Flow Boiling—II: High-CHF Database and Design Equations," *Int. J. Heat Mass Transfer*, **42**, pp. 1429–1456.
- [22] Bouré, J. A., Bergles, A. E., and Tong, L. S., 1973, "Review of Two-Phase Flow Instability," *Nucl. Eng. Des.*, **25**, pp. 165–192.
- [23] Bergles, A. E., 1977, "Review of Instability in Two-Phase Systems," *Two-Phase Flows and Heat Transfer*, S. Kakac, and F. Mayinger, eds., Hemisphere, Washington, Vol. 1, pp. 383–422.
- [24] Yadigaroglu, G., 1981, "Two-phase Flow Instabilities and Propagation Phenomena," *Thermohydraulics of Two-Phase Systems for Industrial Design and Nuclear Engineering*, J. M. Delhaye et al., eds., Hemisphere, Washington, pp. 353–403.
- [25] Todreas, N. E., and Kazimi, M. S., 1990, *Nuclear Systems I*, Hemisphere, New York, Chap. 7.
- [26] Shah, R. K., and London, A. L., 1978, *Laminar Flow Forced Convection in Ducts: A Source Book for Compact Heat Exchanger Analytical Data*, Supl. 1, Academic Press, New York, Chap. 7.
- [27] Collier, J. G., and Thome, J. R., 1994, *Convective Boiling and Condensation*, 3rd edition, Oxford University Press, Oxford, Chap. 2.
- [28] Martinelli, R. C., and Nelson, D. B., 1948, "Prediction of Pressure Drop During Forced-Circulation Boiling of Water," *Trans. ASME*, **70**, pp. 695–702.
- [29] Lockhart, R. W., and Martinelli, R. C., 1949, "Proposed Correlation of Data for Isothermal Two-Phase, Two-Component Flow in Pipes," *Chem. Eng. Process.*, **45**, pp. 39–48.
- [30] Chisholm, D., 1983, *Two-Phase Flow in Pipelines and Heat Exchangers*, Longman, New York, Chap. 7.
- [31] Mukherjee, S., and Mudawar, I., "Pumpless Loop for Narrow Channel and Micro-Channel Boiling," *ASME J. Electron. Packag.*, in press.
- [32] Qu, W., and Mudawar, I., 2002, "Thermal Design Methodology for High-Heat-Flux Single-Phase and Two-Phase Micro-Channel Heat Sinks," *Proceedings of the Eighth Intersociety Conference on Thermal and Thermomechanical Phenomena in Electronic Systems (ITherm 2002)*, C. H. Amon et al., eds., IEEE, pp. 347–359.
- [33] Chen, J. C., 1966, "Correlation for Boiling Heat Transfer to Saturated Fluids in Convective Flow," *I&EC Process Design and Development*, **5**, pp. 322–329.
- [34] Edelstein, S., Perez, A. J., and Chen, J. C., 1984, "Analytic Representation of Convective Boiling Functions," *AIChE J.*, **30**, pp. 840–841.
- [35] Shah, M. M., 1976, "A New Correlation for Heat Transfer During Boiling Flow Through Pipes," *ASHRAE Trans.*, **82**, pp. 66–86.
- [36] Shah, M. M., 1982, "Chart Correlation for saturated Boiling Heat Transfer: Equations and Further Study," *ASHRAE Trans.*, **88**, pp. 185–196.
- [37] Kandlikar, S. G., 1990, "A general Correlation for Saturated Two-Phase Flow Boiling Heat Transfer insider Horizontal and Vertical Tubes," *ASME J. Heat Transfer*, **112**, pp. 219–228.
- [38] Liu, Z., and Winterton, R. H. S., 1991, "A General Correlation for Saturated and Subcooled Flow Boiling in Tubes and Annuli, based on a Nucleate Pool Boiling Equation," *Int. J. Heat Mass Transfer*, **34**, pp. 2759–2766.
- [39] Steiner, D., and Taborek, J., 1992, "Flow Boiling Heat transfer in Vertical Tubes Correlated by an Asymptotic Model," *Heat Transfer Engineering*, **13**, pp. 43–69.